IEEE Access
Multidisciplinary | Rapid Review | Open Access Journal

Received December 5, 2020, accepted December 17, 2020, date of publication January 6, 2021, date of current version January 22, 2021.

Digital Object Identifier 10.1109/ACCESS.2021.3049582

Tumour Nuclear Morphometrics Predict Survival in Lung Adenocarcinoma

NAJAH M. ALSUBAIE[1,2], DAVID SNEAD[3], AND NASIR M. RAJPOOT[2], (Senior Member, IEEE)
[1]Department of Computer Science, College of Computer and Information Sciences, Princess Nourah Bint Abdulrahman University, Riyadh 11564, Saudi Arabia
[2]Department of Computer Science, University of Warwick, Coventry CV4 7AL, U.K.
[3]Department of Histopathology, University Hospitals Coventry and Warwickshire, Coventry CV2 2DX, U.K.

Corresponding author: Najah M. Alsubaie (nmoalsubaie@pnu.edu.sa)

ABSTRACT Providing a quantitative assessment of tumour nuclei would improve decision objectivity and overcome inter and intra-observer variation. In this study, we show that the summary statistics for the whole slide image of nuclear pleomorphism can provide such quantification. We characterise the heterogeneity of lung adenocarcinoma (LUAD) using morphometric features of tumour nuclei. The Cox proportional hazard regression model is employed on a dataset of 78 patients to find the top discriminative features such that there is a strong correlation with patient survival. We find that global nuclear morphometric features, characterised by heatmap statistics, have a significant correlation with overall survival in LUAD ($p < 0.0003$).

INDEX TERMS Digital pathology, deep learning, lung adenocarcinoma, whole slide image.

I. INTRODUCTION

Lung cancer, which accounts for nearly 11% of cancer cases, is among the most prevalent types of cancer worldwide. It is the leading cause of cancer-related deaths at 18%, followed by female breast cancer [1]–[3]. According to the US 2018 cancer statistics, nearly 50% of both male and female lung cancer patients might die because of the disease complications [4]. It has the lowest five-year survival rate, primarily because most of the cases are diagnosed at advanced stages [5], [6].

There are two major categories of lung cancer: non-small cell lung cancer (NSCLC), and small-cell lung cancer (SCLC), comprising 80-85% and 15-20% of lung cancer cases in the UK, respectively [7]. NSCLC has three main subtypes: adenocarcinoma, squamous cell carcinoma and large cell carcinoma. Adenocarcinoma is considered the most prevalent type of NSCLC [8] and has a low five-year survival rate (15%) [9].

Tumour nuclei constitute one of the key tissue components for tumour assessment [8]. Several studies have shown that tumour nuclear morphology is correlated with patient survival. For instance, Nakazato *et al.* [10] find that nuclear size is a significant predictor for lung adenocarcinoma prognosis. Barletta *et al.* [11] and von der Thüsen *et al.* [12] report that nuclear atypia is correlated with adenocarcinoma survival. Kadota *et al.* [13], [14] show that nuclear diameter is an independent factor for poor prognosis in squamous lung cancer.

Generally, studies of tumour nuclear morphology are limited to a number of features such as nuclear size. Findings of these studies are difficult to replicate for comparison and validation purposes due to several reasons. First, the assessment of nuclear morphology requires time and effort. For example, pathologists inspect a small number of visual fields (i.e. regions of interest or ROIs) to assess nuclear features which are then estimated using reference nuclei such as lymphocytes [15]. Second, inter- and intra-observer variability is a common issue in pathology, especially during the assessment of tumour nuclei [16]–[18]. Third, three to four high power fields (HPFs) with distinctive tumour morphology are normally selected for nuclear features evaluation [10]. However, other HPFs may affect the overall distribution of nuclear features. Chalkley counting is another approach for evaluating the volume of a certain histological component relative to the tissue section. In Chalkley counting, a grid is placed on the tissue and then the hot spots areas where there is a high density of the histology component is subjectively chosen from the tumor section [19], [20].

Employing automatic tools to analyse tumour nuclei on whole slide image (WSI) can potentially address the issues above. It can overcome the variability of the assessment by providing an objective method based on the qualitative measures. It can also handle the scalability of data by employing an automatic processing of the whole slide images.

The associate editor coordinating the review of this manuscript and approving it for publication was Easter Selvan Suviseshamuthu.

Several automatic nuclear morphological assessment tools have been proposed. For instance, Yu *et al.* [21] report that textural and morphological features extracted from tumour nuclei and tumour cytoplasm could predict patient survival in LUAD and squamous cell carcinoma. A set of lung cancer cases from The Cancer Genome Atlas (TCGA) [22] and Tissue Microarrays (TMAs) datasets are used. Nuclei are segmented using Otsu threshold [23], and then quantitative features are calculated using CellProfiler [1]. Wang *et al.* [24] perform non-small cell lung adenocarcinoma (NSCLC) subtype classification and survival analysis on TCGA lung cancer dataset. They compute nuclear features such as geometry, intensity statistics and texture to classify lung cancer cases into adenocarcinoma or squamous cell carcinoma and to predict patient survival. Similarly, Wang *et al.* [25] use nuclear orientation, texture, shape and tumour architecture to predict recurrence in NSCLC patients using scanned TMAs. Graph, shape and texture features are shown to be correlated with disease recurrence. Vaidy *et al.* [26] combine radiology and nuclear features extracted from a set of randomly selected visual fields to predict recurrence in early-stage lung cancer. Similar studies are conducted in other types of cancer such as breast cancer [27]–[29], prostate [30], [31], melanoma [32] and others [33], [34].

Most of the proposed automatic nuclear metamorphism scoring models have some of the following limitations. First, using cases from TCGA or TMA databases which might cause a bias towards images where the morphological patterns of lung cancer are definitive. Generally, pathologists review the slides and only identify the most representative regions for the TMAs [21]. Second, analysis of nuclear features might be restricted to a number of ROIs which are selected manually by the expert pathologists.The process of selecting regions of interest is entirely dependent on what looks diagnostically relevant for the pathologist which varies from one pathologist to another [35]. Third, the variation in the morphological abnormality of different types of tumour cells have to be taken into consideration when extracting nuclear features because the morphological abnormality varies for different kinds of cells. For instance,the abnormality in the epithelial tumour cells is characterised as large and irregular size nuclei. However, other type of cells (such as lymphocytes, necrotic, apoptotic etc.) have different morphological characterisation. Hence, comparing statistics between two groups of different types of nuclei might not be valid.

In this study, we aim to overcome the limitations mentioned above. First, we use tissue slides similar to what pathologists encounter in their daily clinical routine. Second, we extract nuclear features from the tumour in WSIs through an automatic parallel processing method at high power (40×). Third, computation of nuclear feature statistics are limited to epithelial tumour nuclei only.

[1]http://cellprofiler.org/

TABLE 1. Summary of clinical and pathological features of the LUAD cohort.

Characteristics of the sample of LUAD patients	
Number of lung adenocarcinoma patients	78
Average age, in years	68
Patient survival	
Average survival, in months	51
Number of censored patients	34 (35%)
Number of patients, by tumour stage	
Stage I	41 (52%)
Stage II	20 (26%)
Stage III	14 (18%)
Unavailable	3 (4%)
Number of patients, by tumour grade	
Well-differentiated tumour	11 (14%)
Moderately-differentiate tumour	27 (35%)
Poorly-differentiated tumour	25 (32%)
Unavailable	15 (19%)
Number of patients, by vascular invasion	
With vascular invasion	39 (50%)
Without vascular invasion	35 (34%)
Unavailable	4 (5%)

Therefore, the main contributions in this paper are threefold: first, to the best of our knowledge, this work is the first to use nuclear features extracted solely from tumour nuclei in haematoxylin and eosin (H&E) WSIs of LUAD. Second, a comprehensive framework is proposed to calculate tumour nuclei features and provide a heatmap for each feature over the WSI. Third, the proposed model assesses the potential correlation between tumour nuclei features and patient survival in LUAD.

II. MATERIALS AND METHODS

Ethics Statement: The dataset included in this study is lung cancer tissue slides which are anonymously collected from the University Hospitals Coventry and Warwickshire (UHCW) NHS Trust in Coventry, UK. The ethics approval for a larger digital pathology study associated with this one is obtained from the National Research Ethics Service North West (REC reference 15/NW/0843).

The dataset includes whole slide images for 78 LUAD patients collected between 2006 and 2014. The slides are H&E stained tissue sections. Clinicopathological variables of patients are extracted from clinical records and pathology reports. Tumour sections are stained with H&E and digitally scanned at 40× using a VL120 Scanner (Omnyx, LLC). All WSIs are reviewed by the pulmonary pathologist (DS). Clinical characteristics of patients are shown in Table 1. In this cohort, the patients are in their 60s, and the majority of patients (52%) are in the early stage of LUAD. Half of the cohort has vascular invasion (50%), and the cohort average overall survival is 51 months. A total of 35% of the patients in our cohort died during the time between 2006 and 2014.

III. THE PROPOSED ANALYSIS FRAMEWORK

The proposed algorithm (See Fig 1) consists of three modules: extracting nuclei, calculating nuclear features, and building the survival model. Broadly, we extract malignant

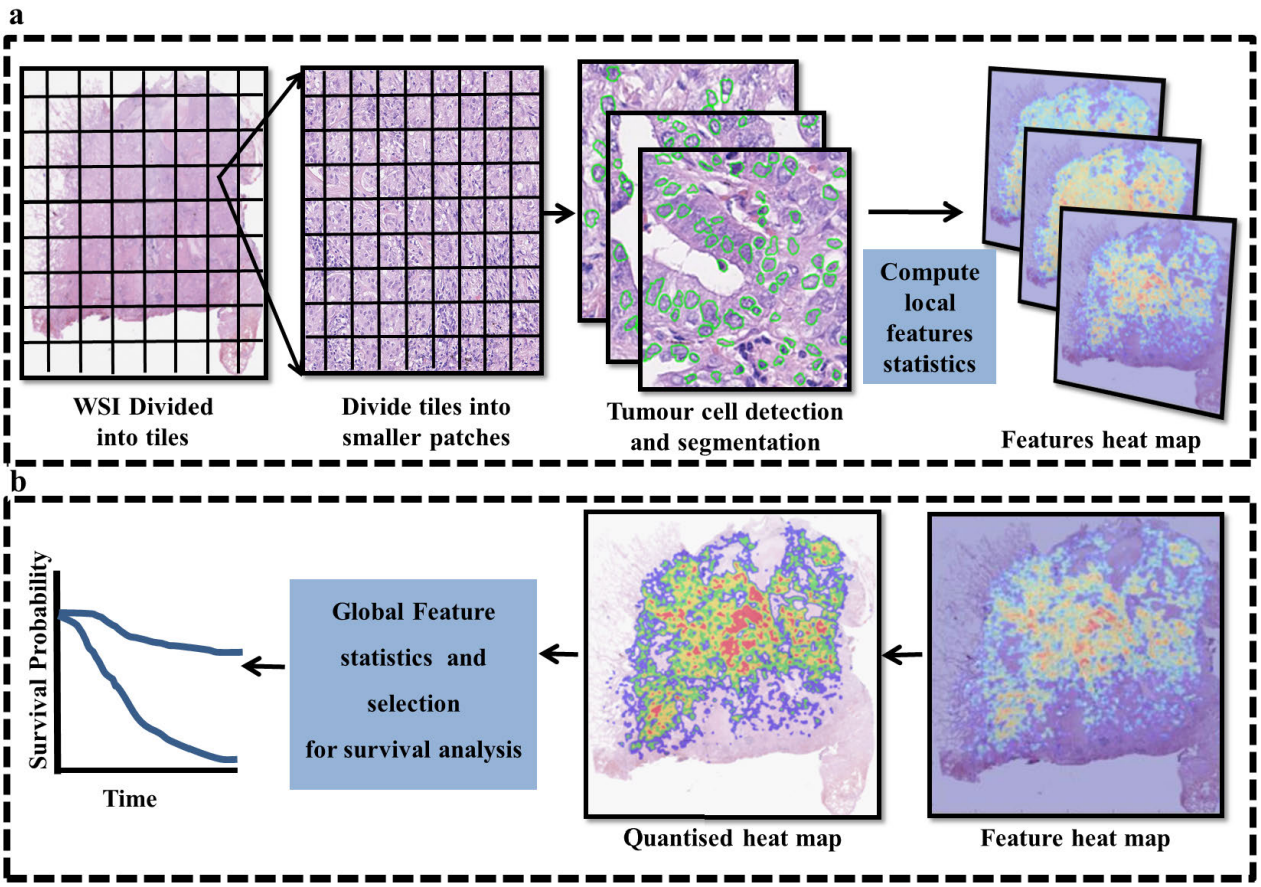

FIGURE 1. Overview of the proposed WSI tumour nuclei analysis framework. (a) Basic WSI processing to allow parallel processing of tiles. Tumour nuclei are detected and segmented. The local morphometric statistics are calculated for each patch to build the final heatmap. (b) Heatmap of each nuclear feature is quantised into discrete intervals. Mean and area for each interval are calculated and added to the final feature list. Finally, features that attain high classification accuracy are selected to build the final survival model.

nuclei by combining nuclei detection and segmentation algorithms. Then, we calculate nuclear features including morphological, textural, and spatial-distribution features. Finally, nuclear feature statistics are computed for the whole slide image and used to find the LUAD overall survival model.

A. FIRST: NUCLEI EXTRACTION

Nuclei extraction method involves tumour nuclei detection and segmentation. For nuclei detection, we train the Spatially Constrained Convolution Neural Network (SC-CNN) to locate centers of tumour nuclei in the WSI. The SC-CNN uses the Gaussian distribution to model the intensity of tumour nuclei where the peak of the Gaussian is the center of the nuclei.

For nuclear segmentation, we utilise the marker-based watershed segmentation algorithm [36]. The details of ground truth generation and nuclear detection and segmentation accuracy are provided in the **Supplementary Materials - Section 1**

B. SECOND: CALCULATING NUCLEAR MORPHOMETRIC FEATURES

We calculated three types of nuclear features: nuclear texture which characterises features such as chromatin distribution and stain colour intensity, nuclear morphology which characterises nuclear size and shape, and nuclear spatial distribution which characterises nuclear arrangement within different areas of the tumour.

The total number of the calculated nuclear features at this stage of the analysis is 115 features. A brief list of the calculated features is given in Table 2. The full list with a detailed description for each feature is given in the **Supplementary Materials - Section 2**

Let $n_i \in \{n_1, \ldots, n_N\}$ be the indices for all the detected nuclei in one sub-image, and p_i in $\{p_1, p_2, ..p_P\}$ be the indices for all sub-images in the whole slide image. For each detected nucleus n_i, we calculate the nuclear feature f_{n_i} (f_{n_i} could be any of the features explained in Table 2). Then, we find the average nuclear feature for the entire sub-image as follow: $f_i = (f_{n_1} + \ldots + f_{n_N})/N$. f_i is then assigned to the corresponding location in the heatmap of the WSI.

Fig2 (a) shows the final heatmap of the tumour cell area, where local standard deviations of the tumour cell area are used to generate the final heatmap. Hotspots are the regions where there is a high variance of the tumour cell area. Fig 2 (b) shows a heatmap for the average distance between tumour cells, where local means of distances between tumour cells are used to generate the final heatmap. The figure shows one

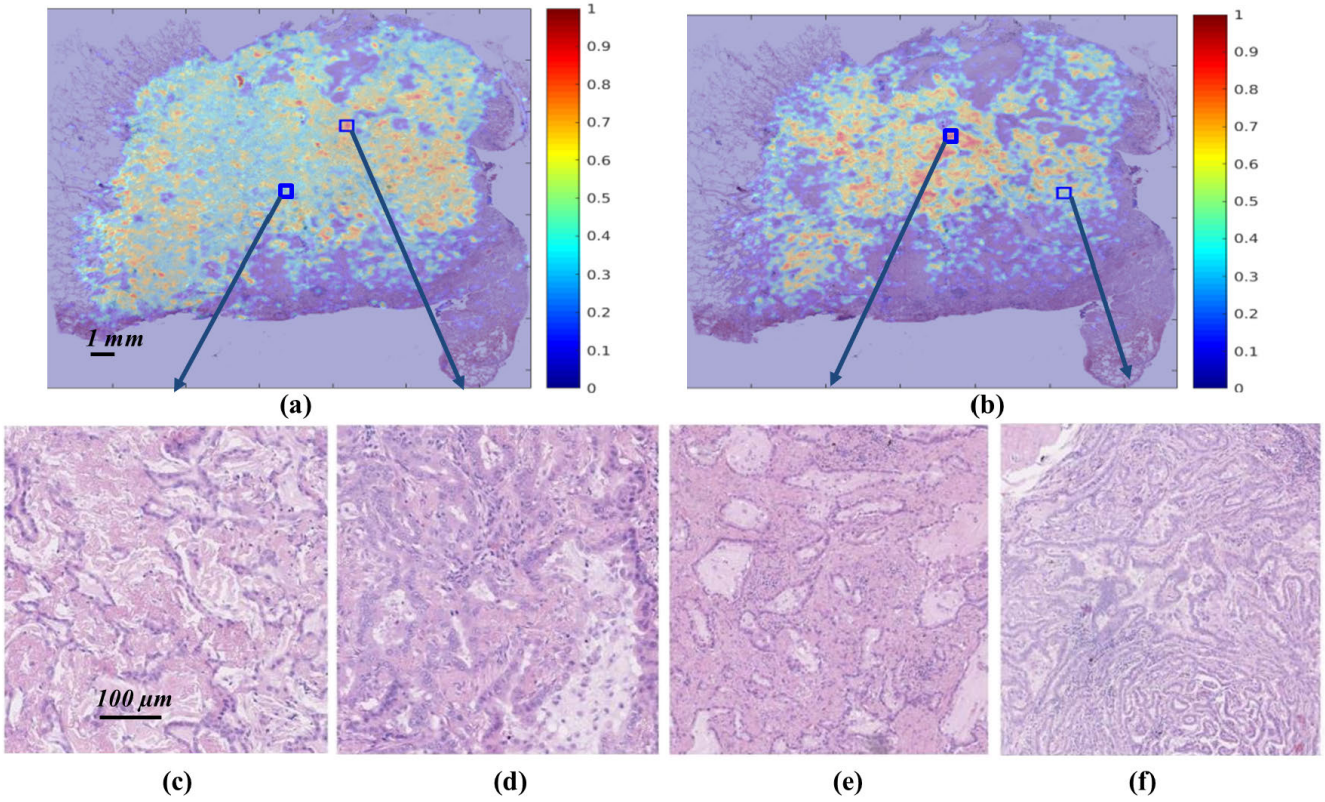

FIGURE 2. (a) Heat map for the standard deviation (SD) of tumour nuclear area. Low value of the heat map (c) represents relatively small variance of the tumour nuclei area; whereas large value of the heat map(d) represents the higher variance of the tumour nuclear area. (b) Heat map for the average distance between tumour nuclei. High value of the heat map represents poorly-differentiated tumour. (e) Low value represents well-differentiated tumour. (e) Glands preserve their overall shape, and nuclei are aligned in relatively uniform spatial distribution. (f) Glands gradually lose their shape, and the distance between tumour nuclei decreases.

hotspot region where glands lose their shape and tumour cells begin to merge.

NUCLEAR FEATURES FOR TUMOUR GRADING

The aim of this section is to reduce the number of calculated features, while keeping the ones that are mostly effective. We train the machine learning algorithm to classify tumour regions into low, intermediate, and high grade, based on nuclear features.

The pathologist (DS) marked regions of interest in eight WSIs and assigned tumour grade (low, intermediate, and high) to each region. The tumour grade is assigned according to the nuclear atypia, which includes nuclear size, texture, and spatial distribution. Then, tumour nuclear features are automatically computed for the selected regions as discussed in the previous section. Next, we train a machine learning algorithm (support vector machine-SVM) using the extracted nuclear features. The SVM is trained to classify tumour regions into low, intermediate, and high grade. More details on this experiment are given in the **Supplementary Material - Section 3**. Last, we selected nuclear features where the classification algorithm achieves high accuracy.

The set of the selected nuclear features that achieve high classification accuracy is given below:

- Nuclear spatial distribution features: average number of links in nuclear clusters and mean inconsistency of nuclear clusters.
- Textural features: kurtosis of nuclear OD image, entropy of the wavelet decomposition of the image, and eight GLCM features [39], [42] namely: auto-correlation, contrast, cluster prominence, dissimilarity, sum of squares, variance, sum variance, and difference of variance.

C. THIRD: BUILD LUAD OVERALL SURVIVAL PREDICTION MODEL USING NUCLEAR FEATURES

Fig 3 shows heatmaps of the same feature for two cases. The figure shows that, for each heatmap, there are distinct levels of intensity, each of which has an average value and area. We use these values to characterise the heatmap of nuclear features as follows: given the heatmap as a 2D matrix where values are normalised in [0, 1], we quantise the heatmap into four levels: minimum (Min) [0, 0.25], above-minimum (Min+) [0.25, 0.5], below-maximum (Max-) [0.5, 0.75], and maximum (Max) [0.75, 1]. We characterised each quantisation level by its mean value and size (the size of the region in pixels divided by the size of the tissue).

TABLE 2. Quantitative nuclear morphometric features.

Feature type	Number	Description
Textural	**84**	A set of nuclear texture features are extracted from both RGB and OD images and wavelet decomposition [37], [38]. These features include: integrated intensity, mean intensity, and intensity deviation. Also, a set of nuclear boundary features [36] are computed, that includes: mean inside boundary intensity, inside boundary intensity deviation, mean outside boundary intensity, outside boundary intensity deviation, boundary saliency, normalised boundary saliency. We also compute mean (OD), variance (OD), skewness (OD), kurtosis (OD), entropy (OD), distance between the centroid and weighted centroid, LBP features, energy, standard deviation and entropy for wavelet decomposition (at the first, second and third levels), gray-level co-occurrence matrix (GLCM) features [39] are also computed for both RGB and OD images.
Morphological	**19**	This includes: area, major axis length, minor axis length,eccentricity, orientation, convex area, filled area, equivalent diameter, solidity, extent, perimeter, convex deficiency, box aspect ratio, radii, compactness, inertia for shape, circularity, elliptical deviation, and mass displacement.
Spatial distribution	**12**	For the graph structure, nuclear centres are considered as the graph nodes, and the distances between nuclei are considered as the graph edges. Then,the following features are extracted: number of nuclei clusters, average number of nuclei per cluster, cluster cophenetic correlation coefficient [40], mean inconsistency [41], average distance between nuclear clusters, number of empty clusters, average number of links in all clusters, average distances between nuclei in all clusters, number of connected nuclei, average number of nodes in all connected nuclei, number of graph edges, and number of nuclei in the patch. These features are summarised as the mean value per patch across the whole slide image.

Thus, each heatmap is characterised by 10 values: mean and variance of the intensity levels in the whole slide image, mean value and size per quantisation level (i.e mean value and size for the regions Min,Min+, Max- and Max). Therefore, each case in our cohort has a feature vector of 1,150 entries (10 global features for each of the 115 tumour nuclei features).

After removing the correlated features, the number of features is reduced to 683. We then analyse the relationship between the final list of the calculated features and patient survival using the Cox proportional hazard model. The **glment** package, which is implemented in **R**, fits a Cox regression model with elastic net penalty by exploring all predictors.

Let x be an $n \times p$ matrix where n is the number of patients and p is the number of predictors (features in this case). Patient survival data are in the form of $(y_1, \delta_1)..(y_n, \delta_n)$, where y is the survival time in months at the last follow up (if δ equals 0, or at the time of death if δ equals 1), and β is the estimated coefficients for each predictor in the model. For simplicity, suppose m is the events of death which are ordered according to the time of occurrence, and denoted by $t_1 < t_2 < \ldots t_m$. Let R_i is the set of individuals who are at risk at time t_i (i.e. those with survival time $y_i \geq t_i$), and j_i is the index of patients who died at time t_i. Then, the inference is based on the partial likelihood for a fixed length vector β of size p.

$$L(\beta) = \prod_{i=1}^{m} \frac{e^{x_{j(i)}^T \beta}}{\sum_{j \in R_i} e^{x_j{}^T \beta}} \quad (1)$$

The Cox model is recommended for regression problems where the number of predictors is greater than the number of observations [43]. Elastic net penalty factor α bridges the gap between the two regularisation paths (lasso and grid). We set α to 0.5 to mix properties of lasso and grid in the predictors selection model [44]. Finally, we selected a feature set that minimises the cross-validation error.

IV. RESULTS AND DISCUSSION

Following the experiment in the previous section, the nuclear features which are best predictors for LUAD survival in our cohort are as follows:

- **Max-** region of the average number of links in nuclear clusters, **Min-** region of mean cluster inconsistency, and **Max-** of the SD of nuclear boundary intensity.
- Mean value of the wavelet coefficient at the second level of the decomposition.

By examining the selected features above, we notice that three out of five of those features are for the quantised regions of the heatmp. This indicates that statistics summarising the heterogeneity of the whole slide nuclear feasters are significant for predicting overall survival in our cohort.

Fig 6 shows the quantised heatmaps using three of the top selected features: the inconsistency of hierarchical clustering, the SD of intensity inside the nuclear boundary, and the average number of links in nuclear clusters. Cases are for long-term survival (first row) and short-term survival (second row). The insets provide an illustration of the nuclear features in both low and high levels of the feature.

Fig 6 (a,b) show the mean inconsistency of nuclear hierarchical clusters. This feature measures the connectivity

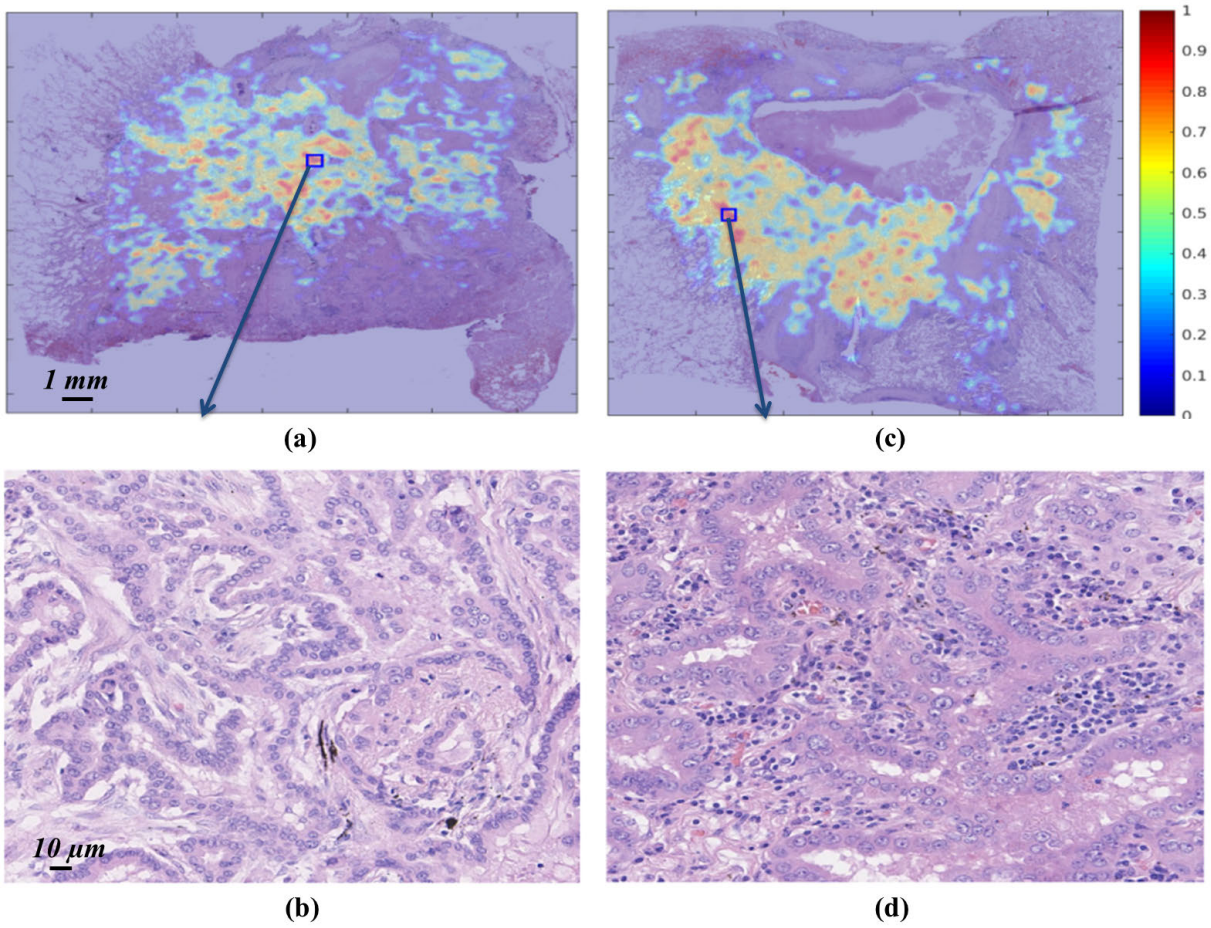

FIGURE 3. Images in (a,c) show the heat maps of the average number of links in nuclear clusters for the well and poorly-differentiated tumours. Small squares in (a,c) are shown with higher magnification (b,d). Images in (b,d) show that the distribution of the feature (i.e. number of links in the nuclear clusters) is variable from one tumour differentiation to another. Notice that the two hotspots in the well and poorly-differentiated tumours have a significant difference in the nuclear spatial distribution.

TABLE 3. Prognostic value of the clinicopathological features and the automatic scoring model according to the univariate Cox proportional hazard regression analysis. HR: hazard ratio, CI: confidence interval.

Clinicopathological Features	β	HR (95% CI for HR)	Wald test	*p-value*
Age	0.69	2 (1-4)	3.8	**0.05**
Tumour site	0.17	1.2 (0.59-2.4)	0.21	0.64
Tumour grade	0.24	1.3 ((0.76-2.1))	0.84	0.36
Stage	0.19	1.2 (0.79-1.8)	0.73	0.39
Vascular invasion	0.94	2.5 (1.2-5.5)	5.6	**0.02**
Automatic scoring model	1.4	3.9 (1.9-8.3)	11	**0.0003**

TABLE 4. Prognostic value of the clinical features and the automatic scoring model according to the multivariate Cox proportional hazard regression analysis. HR: hazard ratio, CI: confidence interval.

Clinical Features	β	HR (95% CI for HR)	*p-value*
Age	0.74	2.09 (0.94 4.62)	0.07
Tumour site	-0.18	0.83 (0.37 1.88)	0.66
Tumour grade	0.39	1.48(0.76 2.88)	0.25
Stage	-0.09	0.91 (0.59 1.42)	0.68
Vascular invasion	0.91	2.47 (0.97 6.34)	0.06
Automatic scoring model	1.78	5.93 (2.43 14.46)	**0.0001**

between two objects in relation to the actual distance between them. Therefore, clusters under one level tend to have lower inconsistency if the distance between them is close to the distance between clusters at lower levels. The bottom insets

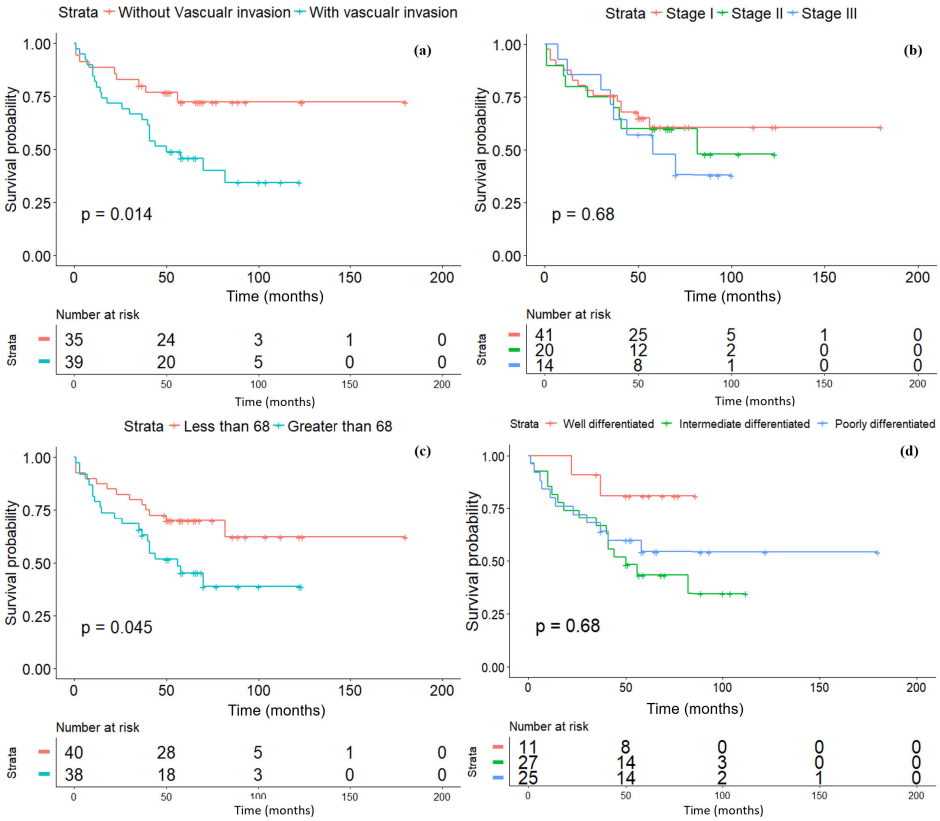

FIGURE 4. Kaplan-Meier survival plots for the clinicopathological factors. *x*-axis is time in months, *y*-axis is the survival probability. (a) Vascular invasion (with and without vascular invasion), (b) tumour stage (Stage I, Stage II, and Stage III), (c) age at diagnosis (age $<$ 68 vs. age $\geq$ 68) and (d) tumour grade (well-differentiated tumour, intermediate-differentiated tumour, and poorly-differentiated tumour).

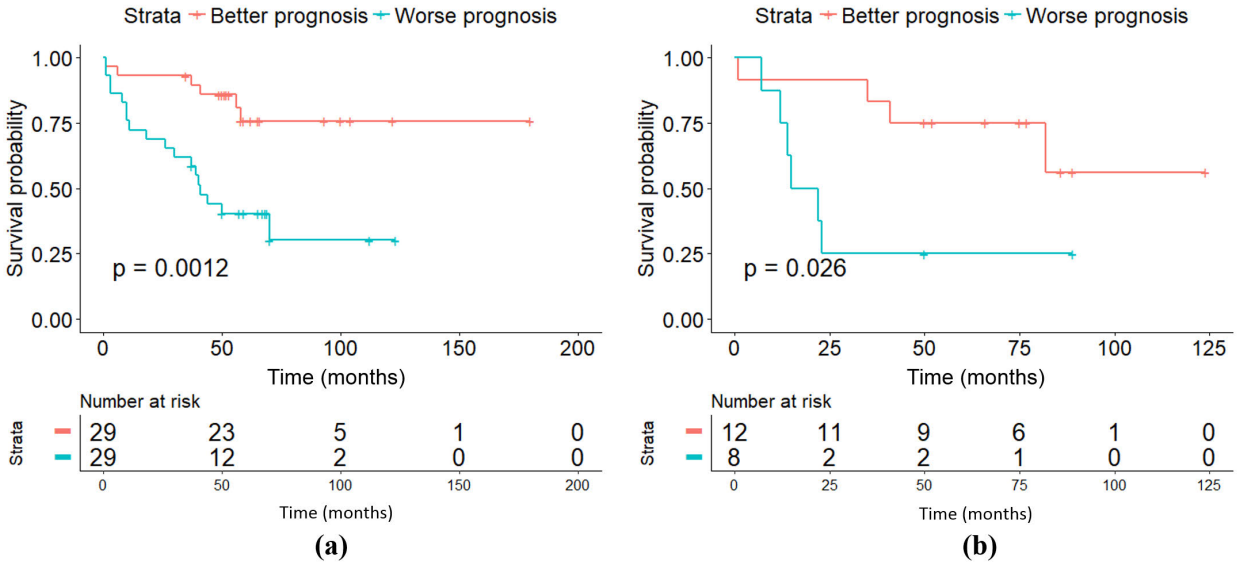

FIGURE 5. Kaplan-Meier survival analysis for autoamtic scoring model. (a) Shows the training set and (b) shows the testing set. *x*-axis is the time in months, *y*-axis is the survival probability. In both sets, the good prognosis group had statistically significant improvement in the overall survival.

(in the first column) show that nuclear clusters short-term survival cases are closer to each other than the nuclear clusters of the long-term survival cases (top insert). In the long-term survival cases, the nuclei are grouped into a distinct glandular structure. The Min+ region is larger in the long-term survival group compared to the short-term survival group.

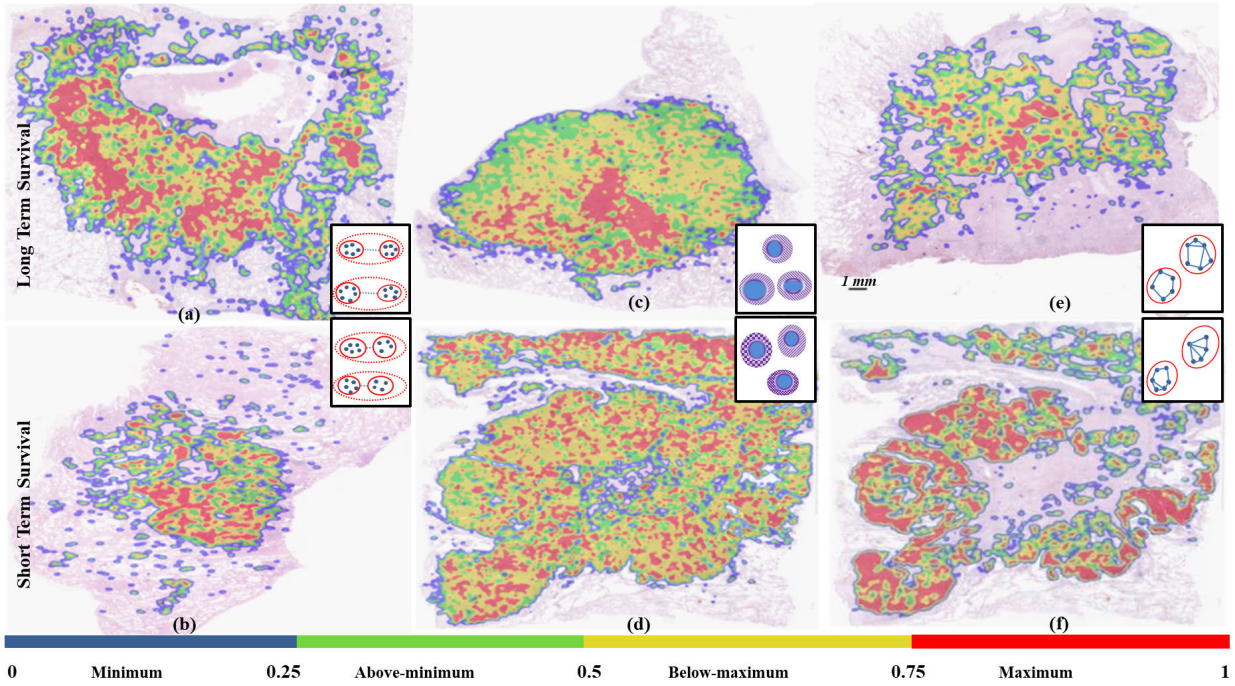

FIGURE 6. Quantised heatmaps using the top selected features, which are correlated with patient survival. The features are as follows (left to right): inconsistency of hierarchical clustering, SD of intensity inside the nuclear boundary, and average number of links in nuclear clusters. Each colour in the heatmap represents one region, and regions are labelled as minimum (Min), above-minimum (Min+), below-maximum (Max-), and maximum Max, as shown in the colour bar at the bottom. Images in the first column (from left) show the mean inconsistency of the nuclear clusters. Images in the second column show the SD of intensity inside the nuclear boundary. Images in the third column show the average number of links in the nuclear clusters.

Fig 6 (c,d) shows the SD of intensity inside the nuclear boundary, which tends to be higher in short-term survival cases than in the long-term survival ones. The Max- region is larger in the long-term survival case than in the short-term survival case. The corresponding insets (in the second column) illustrate the variation in intensity within the nuclear boundary at the high value of the feature (bottom inset) compared to the low value of the feature (top inset).

Fig 6 (e,f) shows the average number of links in nuclear clusters. Short-term survival cases tend to have a high value of this feature, as the tissue begins to lose its structure and nuclei are randomly grouped during the destruction of the tissue. The Max- region is relatively large in the short-term survival cases compared to the long-term survival cases. The corresponding insets (the third column) show that in the low value of the feature (top inset), nuclei are uniformly distributed and grouped into distinct clusters. This creates more distance between the nuclei and hence fewer links between them. The high value of this feature corresponds to the compact distance between tumour cells (bottom inset).

The Cox model estimates patient survival using the function **predict** implemented in the R package. We split the data into two groups. The first group contains 75% of the data, and the second group contains 25%. The first group is used to find the best generalisation parameter λ and lock the Cox object. The Cox object is then used to predict patient survival and to find the threshold that could split the first group into good and bad prognosis. The selected threshold is then tested by predicting patient survival in the second group.

Tables 3 and 4 demonstrate the statistical significance for the clinicopathological factors and the automatic scoring model in predicting patient survival. Table 3 shows the univariate analysis, which examines the association of each independent predictor on patient survival. The automatic scoring model is significantly associated with overall survival (p-value $= 0.0003$). Notably, the standard tumour grading criteria obtained by routine pathological assessment is not strongly associated with patient survival (p-value $= 0.36$). This might be due to the subjective nature of the grading process, which depends on a rough estimation of tumour aggressiveness [45]. Tumour stage on the other hand is one of the significant parameters to predict patient survival. However, due to the small sample size per stage, the model could not find an association between tumour stage and patient survival [46]. However, the Kaplan-Meier survival plots in Fig 4 (b) show that the survival for stage III patients has a considerable decline after 50 months (almost 4 years) of the first diagnosis while stage II has moderate survival and stage I has better survival.

The multivariate analysis in Table 4 demonstrates the impact of the automatic scoring model on the overall survival. The HR for the model is 5.9, which indicates a significant increase (p-value $= 0.0001$) in the hazard after accounting for the other histological factors.

Fig 4 shows that vascular invasion and patient age are significant factors for stratifying the study cohort into a high and low probability of overall survival. The Kaplan-Meier survival plots show that patients without vascular invasion have a higher probability of long overall survival compared to those with vascular invasion. Additionally, younger patients (i.e. age < 68) have a higher probability of longer survival compared to older patients (i.e. age ≥ 68).

Next, we examine the association between the predictions from our model and the actual survival in the cohort using Kaplan-Meier survival plots, Fig 5. The p-values reported in both plots demonstrate the significance of the split between the two groups (good and poor prognoses). Therefore, the lower p-value indicates a higher difference between the survival curves. Thus, cases who are scored as good prognoses by on the nuclear-feature based prediction model might have longer survival and vice versa.

This study has the following limitations: first, the size of the cohort is rather small. Therefore, the automatic scoring model must be validated on a larger number of cases. Second, because of the small cohort, the study is applied to cases from all three stages of LUAD. However, stage plays an important role in predicting survival in LUAD. Therefore, restricting the study to the earlier stages of LUAD (stages I and II) will help to validate the usefulness of WSI tumour nuclear features to predict patient survival.

V. CONCLUSION

Tumour nuclear features are significant indicators of prognosis in LUAD. This study has demonstrated the ability of image-based features extracted from WSIs to stratify LUAD patients with regrade to the overall survival probability. Although nuclear features are well utilised in clinical studies and in the image-based models for other types of cancer, this study is the first that investigated features of tumour nuclei exclusive of other types of nuclei, using the whole tissue section. We show through statistical analysis and Kaplan-Meier survival plots that the tumour nuclear features extracted from the whole tumour are able to predict patient survival in LUAD.

REFERENCES

[1] F. Bray, J. Ferlay, I. Soerjomataram, R. L. Siegel, L. A. Torre, and A. Jemal, "Global cancer statistics 2018: GLOBOCAN estimates of incidence and mortality worldwide for 36 cancers in 185 countries," *CA, Cancer J. Clinician*, vol. 68, no. 6, pp. 394–424, Nov. 2018.

[2] L. Abar, A. R. Vieira, D. Aune, C. Stevens S. Vingeliene, D. A. N. Rosenblatt, D. Chan, D. C. Greenwood, and T. Norat "Blood concentrations of carotenoids and retinol and lung cancer risk: An update of the WCRF–AICR systematic review of published prospective studies," *Cancer Med.*, vol. 5, no. 8, pp. 2069–2083, 2016. [Online]. Available: http://doi.wiley.com/10.1002/cam4.676

[3] A. R. Vieira, S. Vingeliene, D. S. Chan, D. Aune, L. Abar, D. Navarro Rosenblatt, D. C. Greenwood, and T. Norat, "Fruits, vegetables, and bladder cancer risk: A systematic review and meta-analysis," *Cancer Med.*, vol. 4, pp. 136–146, Jan. 2015.

[4] R. L. Siegel, K. D. Miller, and A. Jemal, "Cancer statistics, 2018," *CA, Cancer J. Clinicians*, vol. 68, no. 1, pp. 7–30, Jan. 2018.

[5] P. M. Ellis and R. Vandermeer, "Delays in the diagnosis of lung cancer," *J. Thoracic Disease*, vol. 3, no. 3, p. 183, 2011.

[6] Y.-H. Luo, L. Luo, J. A. Wampfler, Y. Wang, D. Liu, Y.-M. Chen, A. A. Adjei, D. E. Midthun, and P. Yang, "5-year overall survival in patients with lung cancer eligible or ineligible for screening according to US preventive services task force criteria: A prospective, observational cohort study," *Lancet Oncol.*, vol. 20, no. 8, pp. 1098–1108, Aug. 2019. [Online]. Available: Www.thelancet.com/oncology

[7] *National Lung Cancer Audit|RCP London*. Accessed: Apr. 15, 2018. [Online]. Available: https://www.rcplondon.ac.uk/projects/national-lung-cancer-audit

[8] W. D. Travis, E. Brambilla, A. G. Nicholson, Y. Yatabe, J. H. M. Austin, and M. B. Beasley, "The 2015 world health organization classification of lung tumors: Impact of genetic, clinical and radiologic advances since the 2004 classification," *J. Thoracic Oncol.*, vol. 10, no. 9, pp. 1243–1260, 2015.

[9] A. Jemal, R. Siegel, J. Xu, and E. Ward, "Cancer statistics, 2010," *CA, Cancer J. Clinicians*, vol. 60, no. 5, pp. 277–300, Sep. 2010.

[10] Y. Nakazato, Y. Minami, H. Kobayashi, K. Satomi, Y. Anami, K. Tsuta, R. Tanaka, M. Okada, T. Goya, and M. Noguchi, "Nuclear grading of primary pulmonary adenocarcinomas: Correlation between nuclear size and prognosis," *Cancer*, vol. 116, no. 8, pp. 2011–2019, Apr. 2010.

[11] J. A. Barletta, B. Y. Yeap, and L. R. Chirieac, "Prognostic significance of grading in lung adenocarcinoma," *Cancer*, vol. 116, no. 3, pp. 659–669, Feb. 2010.

[12] J. H. von der Thásen, Y. S. Tham, H. Pattenden, A. Rice, M. Dusmet, E. Lim, and A. G. Nicholson, "Prognostic significance of predominant histologic pattern and nuclear grade in resected adenocarcinoma of the lung: Potential parameters for a grading system," *J. Thoracic Oncol.*, vol. 8, no. 1, pp. 37–44, Jan. 2013.

[13] K. Kadota, J.-I. Nitadori, K. M. Woo, C. S. Sima, D. J. Finley, V. W. Rusch, P. S. Adusumilli, and W. D. Travis, "Comprehensive pathological analyses in lung squamous cell carcinoma: Single cell invasion, nuclear diameter, and tumor budding are independent prognostic factors for worse outcomes," *J. Thoracic Oncol.*, vol. 9, no. 8, pp. 1126–1139, Aug. 2014.

[14] K. Kadota, Y. Miyai, N. Katsuki, Y. Kushida, T. Matsunaga, M. Okuda, H. Yokomise, N. Kanaji, S. Bandoh, and R. Haba, "A grading system combining tumor budding and nuclear diameter predicts prognosis in resected lung squamous cell carcinoma," *Amer. J. Surg. Pathol.*, vol. 41, no. 6, pp. 750–760, Jun. 2017.

[15] M. F. Zakowski, "Pathology of small cell carcinoma of the lung.," *Seminars Oncol.*, vol. 30, no. 1, pp. 3–8, 2003.

[16] Y. Nakazato, A. M. Maeshima, Y. Ishikawa, Y. Yatabe, J. Fukuoka, T. Yokose, Y. Tomita, Y. Minami, H. Asamura, K. Tachibana, T. Goya, and M. Noguchi, "Interobserver agreement in the nuclear grading of primary pulmonary adenocarcinoma," *J. Thoracic Oncol.*, vol. 8, no. 6, pp. 736–743, Jun. 2013.

[17] H. F. Frierson, R. A. Wolber, K. W. Berean, D. W. Franquemont, M. J. Gaffey, J. C. Boyd, and D. C. Wilbur, "Interobserver reproducibility of the nottingham modification of the Bloom and richardson histologic grading scheme for infiltrating ductal carcinoma," *Amer. J. Clin. Pathol.*, vol. 103, no. 2, pp. 195–198, Feb. 1995.

[18] W. H. Wolberg, W. N. Street, and O. L. Mangasarian, "Importance of nuclear morphology in breast cancer prognosis," *Clin. Cancer Res.*, vol. 5, no. 11, pp. 3542–3548, 1999.

[19] S. Hansen, D. A. Grabau, F. B. Sørensen, M. Bak, W. Vach, and C. Rose, "The prognostic value of angiogenesis by chalkley counting in a confirmatory study design on 836 breast cancer patients," *Clin. Cancer Res.*, vol. 6, no. 1, pp. 139–146, 2000.

[20] I. Pastushenko, P. B. Vermeulen, S. Vicente-Arregui, G. G. Van den Eynden, R. Alvarez-Alegret, I. Querol, A. Rutten, F. J. Carapeto, L. Y. Dirix, and S. Van Laere, "Peritumoral D2-40 chalkley score independently predicts metastases and survival in patients with cutaneous malignant melanoma," *J. Cutaneous Pathol.*, vol. 42, no. 10, pp. 699–711, Oct. 2015.

[21] K.-H. Yu, C. Zhang, G. J. Berry, R. B. Altman, C. Ré, D. L. Rubin, and M. Snyder, "Predicting non-small cell lung cancer prognosis by fully automated microscopic pathology image features," *Nature Commun.*, vol. 7, no. 1, p. 12474, Nov. 2016.

[22] *The Cancer Genome Atlas—Cancer Genome—TCGA*. Accessed: Apr. 19, 2018. [Online]. Available: https://cancergenome.nih.gov/

[23] N. Otsu, "A threshold selection method from gray-level histograms," *IEEE Trans. Syst., Man, Cybern.*, vol. 9, no. 1, pp. 62–66, Jan. 1979.

[24] H. Wang, F. Xing, H. Su, A. Stromberg, and L. Yang, "Novel image markers for non-small cell lung cancer classification and survival prediction," *BMC Bioinf.*, vol. 15, no. 1, p. 310, 2014.

[25] X. Wang, A. Janowczyk, Y. Zhou, R. Thawani, P. Fu, K. Schalper, V. Velcheti, and A. Madabhushi, "Prediction of recurrence in early stage non-small cell lung cancer using computer extracted nuclear features from digital H&E images," *Sci. Rep.*, vol. 7, no. 1, Dec. 2017, Art. no. 13543.
[26] P. Vaidya, X. Wang, K. Bera, A. Khunger, H. Choi, P. Patil, V. Velcheti, and A. Madabhushi, "Raptomics: Integrating radiomic and pathomic features for predicting recurrence in early stage lung cancer," *Proc. SPIE Med. Imag. Digit. Pathol.*, vol. 10581, Mar. 2018, Art. no. 105810M.
[27] C. Lu, D. Romo-Bucheli, X. Wang, A. Janowczyk, S. Ganesan, H. Gilmore, D. Rimm, and A. Madabhushi, "Nuclear shape and orientation features from H&E images predict survival in early-stage estrogen receptor-positive breast cancers," *Lab. Invest.*, vol. 98, no. 11, pp. 1438–1448, Nov. 2018.
[28] J. Whitney, G. Corredor, A. Janowczyk, S. Ganesan, S. Doyle, J. Tomaszewski, M. Feldman, H. Gilmore, and A. Madabhushi, "Quantitative nuclear histomorphometry predicts oncotype DX risk categories for early stage ER+ breast cancer," *BMC Cancer*, vol. 18, no. 1, p. 610, Dec. 2018.
[29] A. H. Beck, A. R. Sangoi, S. Leung, R. J. Marinelli, T. O. Nielsen, M. J. Van De Vijver, R. B. West, M. Van De Rijn, and D. Koller, "Systematic analysis of breast cancer morphology uncovers stromal features associated with survival," *Sci. Transl. Med.*, vol. 3, no. 108, 2011, Art. no. 108ra113.
[30] G. Lee, R. W. Veltri, G. Zhu, S. Ali, J. I. Epstein, and A. Madabhushi, "Nuclear shape and architecture in benign fields predict biochemical recurrence in prostate cancer patients following radical prostatectomy: Preliminary findings," *Eur. Urology Focus*, vol. 3, nos. 4–5, pp. 457–466, Oct. 2017.
[31] G. Lee, S. Ali, R. Veltri, J. I. Epstein, C. Christudass, and A. Madabhushi, "Cell orientation entropy (core): Predicting biochemical recurrence from prostate cancer tissue microarrays," in *Proc. Int. Conf. Med. Image Comput. Comput.-Assist. Intervent.*, 2013, pp. 396–403.
[32] R. Singh, M. Hanna, C. Liu, and G. Rohde, "Predictive nuclear chromatin characteristics of melanoma and dysplastic nevi," *J. Pathol. Informat.*, vol. 8, no. 1, p. 15, 2017.
[33] K. Sirinukunwattana, D. Snead, D. Epstein, Z. Aftab, I. Mujeeb, Y. W. Tsang, I. Cree, and N. Rajpoot, "Novel digital signatures of tissue phenotypes for predicting distant metastasis in colorectal cancer," *Sci. Rep.*, vol. 8, no. 1, Dec. 2018, Art. no. 13692.
[34] C. Ho, F.-C. Yeh, A. Parwani, and L. Pantanowitz, "Automated grading of renal cell carcinoma using whole slide imaging," *J. Pathol. Informat.*, vol. 5, no. 1, p. 23, 2014.
[35] E. Mercan, S. Aksoy, L. G. Shapiro, D. L. Weaver, T. Brunye, and J. G. Elmore, "Localization of diagnostically relevant regions of interest in whole slide images," in *Proc. 22nd Int. Conf. Pattern Recognit.*, 2014, pp. 1179–1184.
[36] M. Veta, P. J. van Diest, R. Kornegoor, A. Huisman, M. A. Viergever, and J. P. W. Pluim, "Automatic nuclei segmentation in H&E stained breast cancer histopathology images," *PLoS ONE*, vol. 8, no. 7, Jul. 2013, Art. no. e70221.
[37] I. Daubechies, *Ten Lectures Wavelets*, vol. 61. Philadelphia, PA, USA: SIAM, 1992.
[38] S. G. Mallat, "A theory for multiresolution signal decomposition: The wavelet representation," *IEEE Trans. Pattern Anal. Mach. Intell.*, vol. 11, no. 7, pp. 674–693, Jul. 1989.
[39] R. M. Haralick, K. Shanmugam, and I. Dinstein, "Textural features for image classification," *IEEE Trans. Syst., Man, Cybern.*, vols. SMC–3, no. 6, pp. 610–621, Nov. 1973.
[40] R. R. Sokal and F. J. Rohlf, "The comparison of dendrograms by objective methods," *Taxon*, vol. 11, no. 2, pp. 33–40, Feb. 1962.
[41] A. K. Jain and R. C. Dubes, *Algorithms for Clustering Data*. Upper Saddle River, NJ, USA: Prentice-Hall, 1988.
[42] L.-K. Soh and C. Tsatsoulis, "Texture analysis of SAR sea ice imagery using gray level co-occurrence matrices," *IEEE Trans. Geosci. Remote Sens.*, vol. 37, no. 2, pp. 780–795, Mar. 1999.
[43] N. Simon, J. Friedman, T. Hastie, and R. Tibshirani, "Regularization paths for Cox's proportional hazards model via coordinate descent," *J. Stat. Softw.*, vol. 39, no. 5, p. 1, 2011.
[44] H. Zou and T. Hastie, "Regularization and variable selection via the elastic net," *J. Roy. Stat. Soc., Ser. B, Stat. Methodol.*, vol. 67, no. 2, pp. 301–320, Apr. 2005.
[45] K. Inamura, T. Fujiwara, Y. Hoshida, T. Isagawa, M. H. Jones, C. Virtanen, M. Shimane, Y. Satoh, S. Okumura, K. Nakagawa, E. Tsuchiya, and S. Ishikawa, "Two subclasses of lung squamous cell carcinoma with different gene expression profiles and prognosis identified by hierarchical clustering and non-negative matrix factorization," *Oncogene*, vol. 24, no. 47, p. 7105, 2005.
[46] D. G. Beer, S. L. R. Kardia, C.-C. Huang, T. J. Giordano, A. M. Levin, D. E. Misek, L. Lin, G. Chen, T. G. Gharib, D. G. Thomas, and M. L. Lizyness, "Gene-expression profiles predict survival of patients with lung adenocarcinoma," *Nature Med.*, vol. 8, no. 8, p. 816, 2002.

NAJAH M. ALSUBAIE received the Ph.D. degree from the Department of Computer Science, University of Warwick, Coventry, U.K., in January 2019. During her Ph.D., she was a member of the Tissue Image Analytics (TIA) Laboratory. She collaborated with several parties, including Coventry hospitals, where she collected most of the data, and received her training on digital pathology. She is currently an Assistant Professor with Princess Nourah Bint Abdulrahman University, Riyadh, Saudi Arabia. She has published several articles in histology image analysis and has served as a reviewer for several articles.

DAVID SNEAD is currently a Consultant Pathologist with the University Hospitals Coventry and Warwickshire and a Professor of Pathology Practice with the University of Warwick. He has been in post at Coventry for 20 years. He is the Founding Director of PathLAKE, one of the five Innovate U.K. funded centres of excellence for the development of artificial intelligence in digital pathology and radiology. He is an international expert in the use of digital pathology having led Coventry to be one of the first hospitals in Europe, to switch to digital pathology for routine diagnosis. His team has published the world's largest validation study on the use of digital pathology, and which was awarded the 2016 Roger Cotton Prize for best paper in Histopathology. Prior to leading PathLAKE, he was with UHCW, for many years to the clinical lead for cellular pathology. This experience has given him a unique understanding of how innovative AI-based solutions can be deployed to address the major challenges facing cellular pathology department across the NHS.

NASIR M. RAJPOOT (Senior Member, IEEE) received the Ph.D. degree in computer science from the University of Warwick, in 2001.

He is currently a Professor of Computational Pathology with the University of Warwick and an Honorary Scientist with the Department of Pathology, University Hospitals Coventry and Warwickshire (UHCW) NHS Trust. Prior to completing his Ph.D., he was a Postgraduate Research Fellow with the Applied Math Program at Yale University, USA, from 1998 to 2000, and a Systems Engineering Fellow at PIEAS, Pakistan, from 1994 to 1996. He has been the Director and the Founding Head of the Tissue Image Analytics (TIA) laboratory, University of Warwick, since 2012, and also the Co-Director of the recently funded £15m PathLAKE Centre of Excellence on AI in Pathology, since January 2019. The focus of current research in TIA Laboratory led by him is on developing novel computational pathology algorithms with applications to computer-assisted grading of cancer and image-based markers for prediction of cancer progression and survival. He has been active in the digital pathology community for over a decade and has delivered over 50 invited and keynote talks, since 2015, at various national and international events and institutions.

Prof. Rajpoot is a member of the Association of the Computing Machinery (ACM), The British Association for Cancer Research (BACR), the European Association for Cancer Research (EACR), and the American Society of Clinical Oncology (ASCO). He was recently awarded the Wolfson Fellowship by the U.K. Royal Society and the Turing Fellowship by the Alan Turing Institute, the U.K.'s National Data Science Institute. He served as the President of the European Congress on Digital Pathology (ECDP), which took place at Warwick, in April 2019. Previously, he served as the General Chair for the U.K. Medical Image Understanding and Analysis (MIUA) Conference, in 2010, and as the Technical Chair for the British Machine Vision Conference (BMVC), in 2007. He has co-chaired several meetings in the histology image analysis (HIMA) series, since 2008, and served as a Founding PC Member of the SPIE Digital Pathology meeting, since 2012.